Int. J. Electrochem. Sci., 13 **(2018)** 4661 – 4669, doi: 10.20964/2018.05.09

International Journal of
ELECTROCHEMICAL
SCIENCE
www.electrochemsci.org

Morphology Control of a Nanoporous Nickel/Cobalt Double Hydroxide for Supercapacitor Electrode Materials using Halides

Yuqing Yang, You Yang, Hongqing Wang, Rui Xie, Guoping Wang[*]

College of Chemistry and Chemical Engineering, University of South China, Hengyang, Hunan 421001, China
[*]E-mail: wgpcd@aliyun.com

Received: 15 January 2018 / *Accepted:* 28 February 2018 / *Published:* 10 April 2018

Nickel/cobalt double hydroxides with sphere-like nanoflowers and nanoporous structures were controllably prepared by introducing halide ions into the reaction system. The morphology and structure of the composites were characterized by X-ray diffraction, scanning electron microscope, infrared spectra and Brunauer-Emmett-Teller method. Halides, especially bromide, can dramatically affect the morphology of the crystal aggregates, and some morphology-dependent electrochemical properties are found. Nickel/cobalt double hydroxide, prepared in the presence of potassium bromide, exhibits excellent electrochemical performance. The composite's specific capacitance can reach 2630 F g^{-1} at a current density of 1 A g^{-1}. Even at 8 A g^{-1}, the composite can still retain 80.7% of its capacitance, which is much higher than that of nickel/cobalt double hydroxide prepared in the absence of bromide (68.6%).

Keywords: Nickel/cobalt double hydroxide; Halide; Morphology control; Electrochemical supercapacitor

1. INTRODUCTION

An electrochemical supercapacitor's wide application prospects have attracted significant attention throughout the world because of its long cycle life, high power density, and bridging function for the power/energy gap between traditional dielectric capacitors and batteries/fuel cells [[1-3]. However, to date, electrochemical supercapacitors still suffer from a lower energy density. Researchers have tried to improve the energy density of supercapacitors by using electrode materials with a high specific capacitance and power density. Electrode materials play a very important role in the

performance of supercapacitors. The investigated electrode materials can be classified into three major types: (1) highly porous activated carbon, (2) electronically conducting polymers, and (3) metal oxides/hydroxides [4].

Serving as electrode materials for supercapacitors, metal oxides/hydroxides have received increasing interest due to their high specific capacitance, low cost, rich reserve of resources and environmental-friendliness [[5, 6]. Regrettably, their low electronic and ion conductivities restrict their practical applications in high-performance supercapacitors. During recent years, researchers have attempted to overcome the shortcomings of these electrode materials by optimizing their morphology, specific surface area, pore size and pore size distribution. For example, nickel–cobalt double hydroxide microspheres have been synthesized and exhibit a three-dimensional structure with hollow interior and hedgehog-like exterior structures. Such a special structure greatly benefits the electrochemical properties of nickel–cobalt double hydroxide. The specific capacitance can reach 2275.5 F g^{-1} at a current density of 1 A g^{-1} [7]. Nickel–cobalt double hydroxide nanosheets, which have been successfully synthesized by means of an epoxide precipitation route, display a specific capacitance of 2548 F g^{-1} at a current density of 0.9 A g^{-1} and remain at 1587 F g^{-1} even at 35.7 A g^{-1} [8]. In addition, nanofibrous α-Ni-Co$(OH)_2$ with a macroporous nickel-shell has been synthesized by using polyethylene glycol as a structure directing reagent. The prepared α-Ni-Co$(OH)_2$@NS electrode shows a specific capacitance as high as 2962 F g^{-1} at 5 mV s^{-1} [9].

The morphology control of materials has aroused growing concern due to the achievements in tuning the catalytic activity and selectivity by modifying the exposed facets of the nanocrystals in a series of catalytic reactions [10]. By analogy, in electrochemical fields such as supercapacitors, developing metal oxide/hydroxide composites with an appropriate morphology may also be an effective approach to further increase the electrochemical performance of an electrode material and may become a new trend for supercapacitor electrode materials. To date, little work has been conducted to evaluate the effects of nanoparticle shape on the electrochemical performance of an electrode material. Many studies are necessary. Specifically, realizing the morphology-controlled synthesis of metal oxides/hydroxide with nanostructures through a convenient, mild, environmentally friendly, and cost-effective route remains a large challenge.

When a reaction is under thermodynamic control to approximate the stable product, the formation of single-crystal seeds can be considered in the context of Wulff's theorem, which attempts to minimize the total interfacial free energy of a system with a given volume [11]. According to Wulff's theorem, if the interfacial free energy of a reaction system is changed, the morphology of the materials can be expected to be altered.

Based on the above idea, in this paper, nickel/cobalt double hydroxides (Ni/Co-DH) with nanoflower spherical shapes were synthesized by using halides (KBr and KI) to change the interfacial free energy of the reaction system [12]. Interestingly, halides can remarkably affect the shape and size of metal nanoparticles, and the electrode materials obtained in the presence of KBr and KI show excellent electrochemical performance.

2. EXPERIMENTAL

2.1. Material synthesis

Two types of morphology-controlled Ni/Co-DH were synthesized by using a simple chemical precipitation method in the presence of KBr or KI. For comparison, blank Ni/Co-DH was also prepared with a similar process, except for the absence of halide ions. First, 0.582 g of $Co(NO_3)_2 \cdot 6H_2O$ and 0.582 g of $Ni(NO_3)_2 \cdot 6H_2O$ were dissolved in 60 ml deionized water. Then, 0.952 g KBr or 1.328 g KI was added into the above mixtures. Afterwards, ammonia hydroxide was added dropwise to the above solution until the pH reached 8.0. The solution was stirred at room temperature for 4 hours. After 6 hours of ageing, the precipitates were filtered and washed with deionized water and alcohol several times. The product was finally dried at 80 °C under vacuum for 12 h. Hereafter, the as-prepared samples were denoted as Ni/Co-DH-KBr, Ni/Co-DH-KI and Ni/Co-DH.

2.2. Characterization

The surface morphologies of the prepared samples were observed using scanning electron microscope (SEM, JSM-7500F, Japan). The structure and phase analysis of the samples were characterized by X-ray diffraction (XRD, Bruker D8 advance X-ray diffractometer, Germany) with Cu Kα radiation at 40 kV, and the detected diffraction angle was scanned from 5° to 90° with a scan speed of 10° min^{-1}. The component was analysed by infrared spectra (FTIR, IRPrestige-21 FTIR, Shimadzu, Japan). The specific surface area and the pore size distribution were determined by the Brunauer-Emmett-Teller method (BET, 3H-2000PM2 volumetric adsorption analyser, Beijing, China) using nitrogen as the adsorption-desorption gas at 77.3 K.

2.3. Electrochemical evaluation

The electrochemical performance of Ni/Co-DH was characterized by cyclic voltammetry (CV), galvanostatic charge/discharge (GCD) and electrochemical impedance spectra (EIS) performed on a CHI660E electrochemical workstation (Huakeputian Beijing, China) with a conventional three-electrode system. A Pt sheet and a Hg/HgO electrode were utilized as the counter electrode and reference electrode, respectively, and Ni/Co-DH-coated glassy carbon (geometric surface area of 0.07 cm^2) was used as the working electrode. All the measurements were conducted in a 6.0 M KOH electrolyte solution at room temperature (23±2 °C) and atmospheric pressure.

The working electrode was prepared as follows: 9.0 mg Ni/Co-DH and 1.0 mg carbon nanotubes were ultrasonically dispersed in 5.0 ml isopropanol for 10 min, and then 5.0 μL of this dispersion ink was pipetted gradually onto a pretreated glassy carbon electrode with a microsyringe. After drying, 5.0 μL of the diluted Nafion® solution (0.1 wt%, Aldrich) was used to cover this coated glass carbon electrode to form a uniform electrode layer for the electrochemical measurements.

3. RESULTS AND DISCUSSION

3.1. Materials characterization

For morphologies of the prepared samples, Fig. 1 shows the SEM images of Ni/Co-DH, Ni/Co-DH-KBr and Ni/Co-DH-KI. It can be seen that the thin flakes of Ni/Co-DH are stacked disorderly and randomly. Almost no mesopores are observed in Ni/Co-DH. However, both Ni/Co-DH-KBr and Ni/Co-DH-KI exhibit sphere-like nanoflower shape, and dozens of nanometre pores between the thin flakes are very clear. Particularly, Ni/Co-DH-KBr shows a more obvious sphere-like shape, a smaller aggregate size and a clearer mesoporous structure than does Ni/Co-DH-KI [13]. The average size of a Ni/Co-DH-KBr aggregate is approximately 300 nm. According to the above phenomenon, it can be concluded that the addition of a halide, especially bromide, plays a critical role in the formation of crystal aggregates [14].

Halide ions may adsorb onto a particular facet and alter the surface free energy of the Ni/Co-DH seeds, altering the order of the surface free energies of the different facets, which inhibits further growth in a specific direction [12, [15-17]. In this experiment, Br^- and I^- may favour the stabilization of the (100) facet and induce the (111) facet as a common edge to contact with neighbouring crystals. As a result, the desired morphology of the aggregate is selectively generated, and a large number of Ni/Co-DH flaky nanocrystals share the (111) facet to form sphere-like nanoflowers [11].

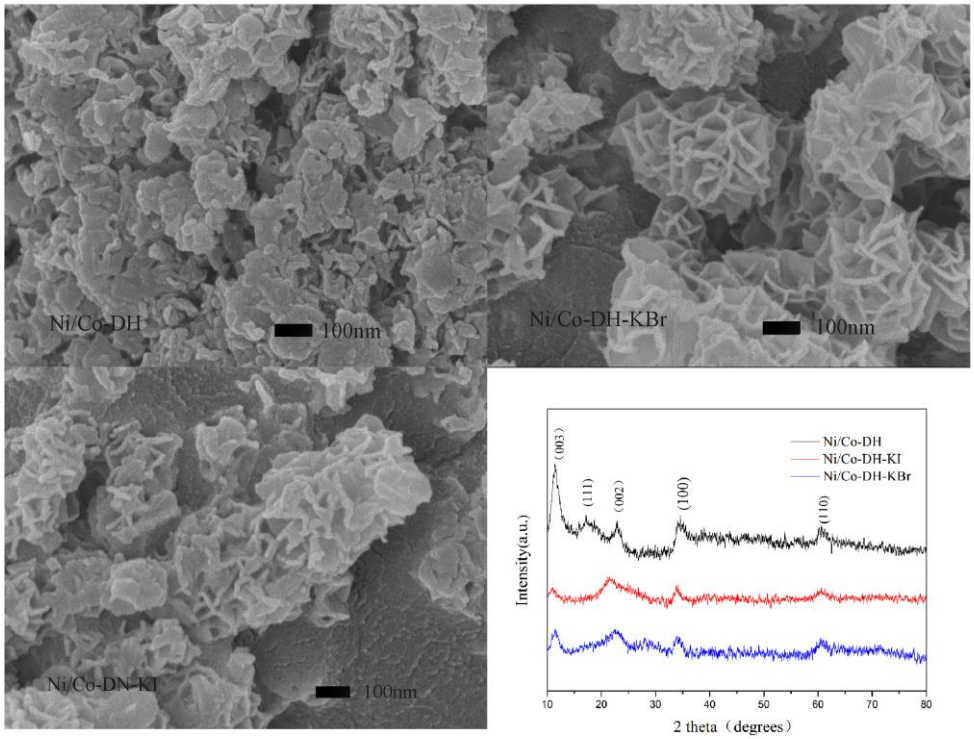

Figure 1. SEM images and XRD patterns of Ni/Co-DH, Ni/Co-DH-KBr and Ni/Co-DH-KI

The XRD patterns of Ni/Co-DH, Ni/Co-DH-KBr and Ni/Co-DH-KI are depicted in Fig. 1. Due to the similar sizes of Ni^{2+} and Co^{2+}, they can replace each other in the crystal. The characteristic peaks

of α-$Ni(OH)_2$ (JCPDS:38-0715) and α-$Co(OH)_2$ (JCPDS:46-0605) are overlaid to form broad peaks. All of the three types of materials present four obvious peaks, which are indexed to the (003), (002), (100) and (110) facets. These data imply that the three binary hydroxides almost exhibit some similar crystalline structure [18]. Nevertheless, it should be noted that compared with Ni/Co-DH-KBr and Ni/Co-DH-KI, Ni/Co-DH presents a unique characteristic peak indexed to the (111) facet. This peak is attributed to the addition of the halide. In Ni/Co-DH-KBr and Ni/Co-DH-KI, the halide ions promote the sharing of the (111) facets as a common edge of the plurality of the crystal units to form sphere-like nanoflowers [19]. As the result, the (111) facets are covered in the centre of the flower, resulting in the loss of the characteristic peak of the (111) facets [20].

Fig. 2 shows the FTIR spectra of Ni/Co-DH, Ni/Co-DH-KBr and Ni/Co-DH-KI. The peaks centred at 1385 and 852 cm^{-1} correspond to the v3 and v2 vibrational modes with the D_{3h} symmetry of NO^{3-}, implying the presence of intercalated NO^{3-} in the three samples. The absorption of O-H stretching of the intermediate layer H_2O molecules appears at approximately 3500 cm^{-1}, and the IR peak of the bending mode of H_2O molecules is located at approximately 1625 cm^{-1}. The peaks at approximately 672 and 528 cm^{-1} correspond to Ni-O and Co-O stretching vibrations, respectively. With the addition of halide ions, Ni/Co-DH-KBr and Ni/Co-DH-KI present a special peak at 1493 cm^{-1}, suggesting the presence of intercalated halide ions in the interlayer space of nickel/cobalt double hydroxide [21].

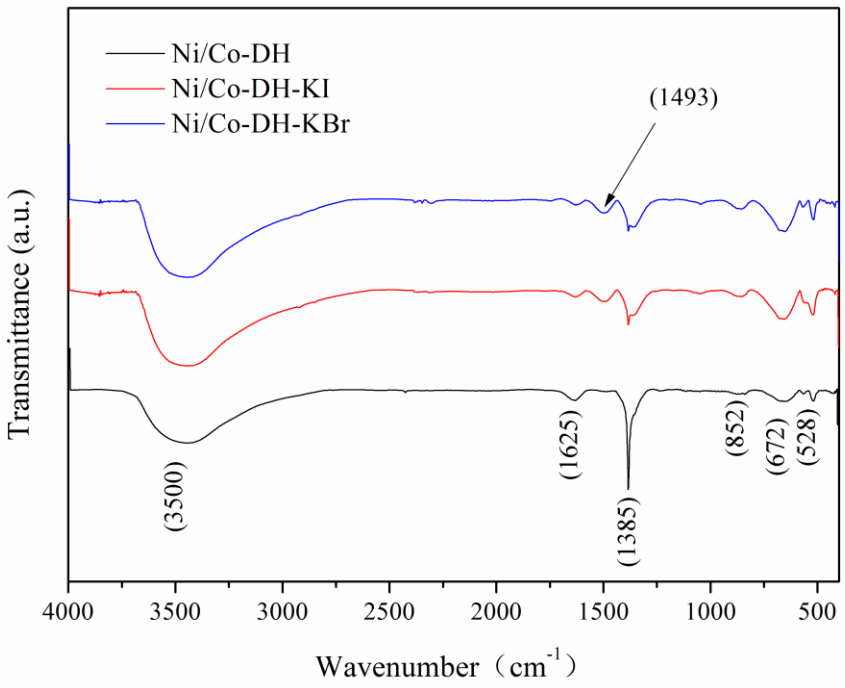

Figure 2. FTIR spectra of Ni/Co-DH, Ni/Co-DH-KBr and Ni/Co-DH-KI

The surface area and pore size play a crucial role in electrochemical performance. Fig. 3 presents the nitrogen adsorption-desorption isotherms and pore size distributions of the nickel/cobalt double hydroxide. All of the Ni/Co-DH samples exhibit typical IV isotherms with H3-type hysteresis

loops (P/P_0> 0.45), indicating the presence of mesopores [22]. The specific surface area of Ni/Co-DH, Ni/Co-DH-KBr and Ni/Co-DH-KI are 52.134, 60.973 and 53.256 m^2 g^{-1}, respectively, and their average pore sizes are 30.828, 29.843 and 30.231 nm, respectively. The corresponding pore volumes are 0.402, 0.455 and 0.403 cm^3 g^{-1}.

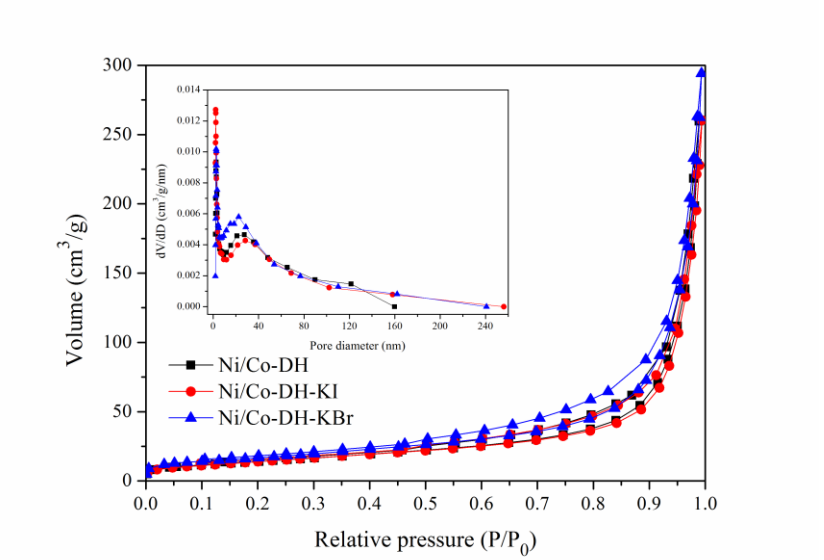

Figure 3. Nitrogen adsorption-desorption isotherms and pore size distribution profiles (inset) of Ni/Co-DH, Ni/Co-DH-KBr and Ni/Co-DH-KI

3.2. Electrochemical properties

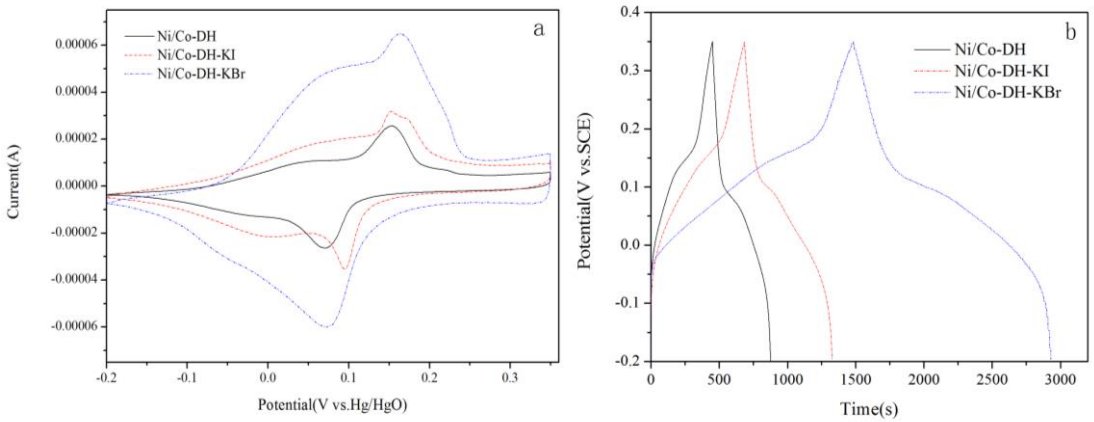

Figure 4. (a) CV curves of Ni/Co-DH, Ni/Co-DH-KBr and Ni/Co-DH-KI at 1 mV s^{-1}. (b) Charge-discharge curves of Ni/Co-DH, Ni/Co-DH-KBr and Ni/Co-DH-KI at 1 A g^{-1}

The cyclic voltammograms of Ni/Co-DH, Ni/Co-DH-KBr and Ni/Co-DH-KI at 1 mV s^{-1} are shown in Fig. 4a. All of them have a significant redox peak. The integrated areas of Ni/Co-DH-KBr and Ni/Co-DH-KI are larger than that of Ni/Co-DH, indicating that the Ni/Co-DH-KBr and Ni/Co-DH-KI electrodes possess higher specific capacitance values. Especially, the Ni/Co-DH-KBr electrode attains a specific capacity as high as 2690 F g^{-1}. In the charge-discharge curves (Fig. 4b), all of the curves have a relatively symmetrical charge and discharge curve, indicating their excellent

reversibility. Among them, the Ni/Co-DH-KBr electrode has the longest charge-discharge plateau. The specific capacitance of Ni/Co-DH-KBr obtained from the charge and discharge curve reaches 2630 F g^{-1} at a current density of 1 A g^{-1}. This density may be attributed to the Ni/Co-DH-KBr sphere-like morphology, higher specific surface areas and higher pore volumes which greatly improves the faradaic redox reaction and mass transfer and improve the electrochemical performance [17, 23]. The sphere-like nanoflowers may increase the specific surface area and optimize the pore structure of the material, exposing more electrochemical active points for a redox reaction. Meanwhile, the higher pore volume and clear mesopores may facilitate the storage and transportation of electrolyte ions within the interior space of the electrode material [24, 25]. This in turn may result in a higher utilization of the electrode materials and a higher specific capacitance. The impedance offers further evidence.

Generally, a semicircle in the high frequency region of impedance plots indicates the resistance of the charge transfer in the material, and the straight line in the low frequency region is related to the diffusion rate of the electroactive component of the electrolyte. In Fig. 5, compared with Ni/Co-DH, Ni/Co-DH-KBr and Ni/Co-DH-KI present a straight line with a higher slope at a low frequency, implying their low diffusion resistance. This phenomenon may result from the difference in pore structure as described above. In addition, Ni/Co-DH-KBr shows the smallest semicircle, implying that this material demonstrated the lowest resistance to charge transfer, which is obviously related to its higher specific surface area and higher pore volume. The higher pore volume means that Ni/Co-DH-KBr can store a larger amount of electrolyte and in turn shorten the transportation distance of the ions. This shorter distance suggests a lower reaction resistance [26].

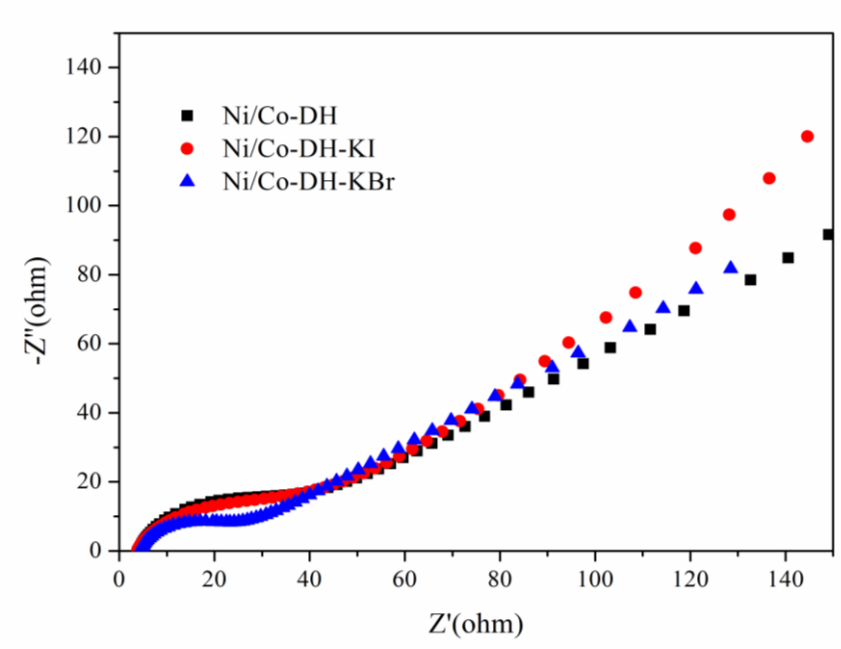

Figure 5. Impedance plots of Ni/Co-DH, Ni/Co-DH-KBr and Ni/Co-DH-KI

The specific capacitances of Ni/Co-DH, Ni/Co-DH-KBr and Ni/Co-DH-KI decreased with an increase in the current density (Fig. 6). Without any doubt, increasing the current density makes

electrolyte ion diffusion and impregnation into the interior space of electrode material difficult, leading to a decrease in the electrochemical accessible specific surface area and then a decrease in the specific capacitance [27]. Nevertheless, Ni/Co-DH-KBr shows a better rate performance. At a current density of 8 A g^{-1}, Ni/Co-DH-KBr can retain an 80.7% capacitance of 1 A g^{-1}, which is much higher than that of Ni/Co-DH-KI (68.6%) and Ni/Co-DH (72.0%). This finding is attributed to its higher pore volume, which decreases the diffusion distance of the electrolyte and readily meets the need of the electrolyte at a higher scan rate.

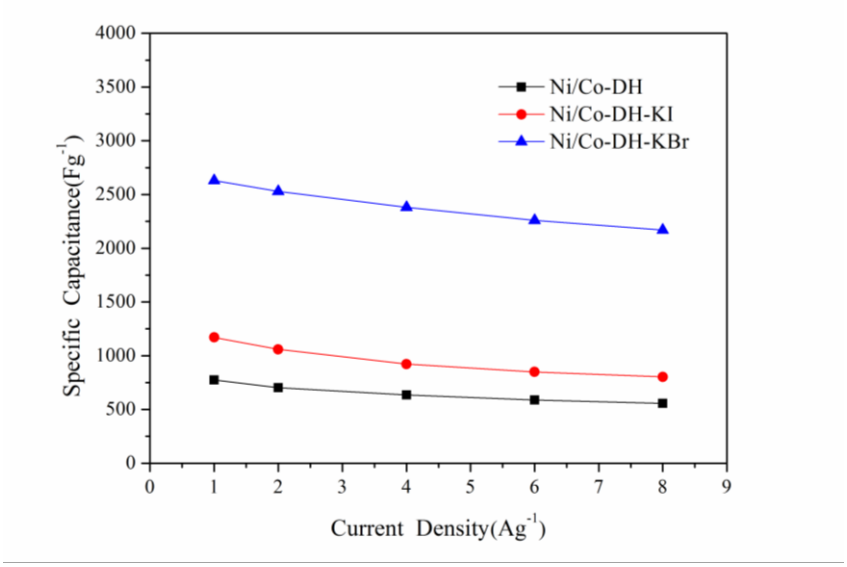

Figure 6. Specific capacitance of Ni/Co-DH, Ni/Co-DH-KBr and Ni/Co-DH-KI at different current densities

4. CONCLUSIONS

Nickel/cobalt double hydroxides with a sphere-like nanoflower shape were controllably synthesized by introducing halides (KBr and KI) as a morphology directing reagent into the reaction system. Halide adsorption onto a particular facet and altering the surface free energies of the Ni/Co-DH seeds can induce the desired aggregate morphology. Ni/Co-DH-KBr and Ni/Co-DH-KI possess a sphere-like shape, a smaller aggregate size and a clearer mesopore structure. Particularly, Ni/Co-DH-KBr presents a more obvious sphere-like shape, a higher specific surface area, a smaller average pore size and a higher pore volume. The nanoflower sphere increases the specific surface area and optimizes the pore structure of the material, exposing more electrochemical active points for a redox reaction. The higher pore volume and clear mesopores facilitate the storage and transportation of electrolyte ions within the interior space of the electrode material. These factors in turn result in a higher utilization of the electrode materials and a higher specific capacitance. The Ni/Co-DH-KBr electrode shows a better rate performance compared with that of the other Ni/Co-DH electrodes. When the current density increases from 1 to 8 A g^{-1}, Ni/Co-DH-KBr can retain 80.7% of its capacitance, which is much higher than that of Ni/Co-DH-KI (68.6%) and Ni/Co-DH (72.0%). The study provides a promising approach for the controllable synthesis of materials with a given morphology and nanopores.

ACKNOWLEDGEMENTS
The work was supported by the Research Foundation of Education Bureau of Hunan Province, China (grant number 15B200), and the Natural Science Foundation of Hunan Province, China (grant number 2016JJ3105).

References

1. G. Wang, L. Zhang and J. Zhang, *Chem. Soc. Rev.*, 43 (2012) 797.
2. S. G. Kandalkar, D. S. Dhawale, C. K. Kim and C. D. Lokhande, *Synth. Met*., 160 (2010) 1299.
3. Z. Hu, L. Mo, X. Feng, J. Shi, Y. Wang and Y. Xie, *Mater. Chem. Phys*., 114 (2009) 53.
4. G. Wang, L. Zhang, J. Kim and J. Zhang, *J. Power Sources*, 217 (2012) 554.
5. T. Yan, R. Li, T. Yang and Z. Li, *Electrochim. Acta*, 152 (2015) 530.
6. U. M. Patil, J. S. Sohn, S. B. Kulkami, S. C. Lee and H. G. Park, *ACS Appl. Mater. Interface*, 6 (2014) 2450.
7. T. Yan, Z. Li, R. Li, Q. Ning, H. Kong and Y. Niu, *J. Mater. Chem*., 22 (2012) 23587.
8. M. Wang, J. Xue, F. Zhang, W. Ma and H. Cui, *J. Nanopart. Res*., 17 (2015) 106.
9. R. B. Marichi, V. Sahu, S. Lalwani, M. Mishra, G. Gupta and R. K. Shama, *J. Power Sources*, 325 (2016) 762.
10. A. X. Yin, X. Q. Min, Y. W. Zhang and C. H. Yan, *J. Am. Chem. Soc*., 133 (2011) 3816.
11. Y. X. Prof, Y. X. Dr, B. L. Dr, Sara and E. Skrabalak. Dr, *Angew. Chem*., 48 (2009) 335.
12. Q. Y. Li, R. N. Wang, Z. R. Nie, Q. Wei, Z, H, Wang, *J. Alloy Compd.*, 496 (2010) 300.
13. Y. Luo, G. Duan, G. Li, *J. Solid State Chem*., 180 (2007) 2149.
14. H. H. Tai, A. Heejoon Koo and B. H. Chung, *J. Phys. Chem*. C, 111 (2007) 1123.
15. Y. J. Wang, N. Zhao, B. Fang, H. Li, X. T. Bi and H. Wang, *Chem. Rev.*, 115 (2015) 3433.
16. Y. J. Xiong, H. G. Cai, B. J. W, J. G. Wang, M. J. K and Y. N. Xia, *J. Am. Chem. Soc*., 129 (2007) 3665.
17. X. Ni, H. Zheng, X. Xiao, X. Jin, G. Liao, *J. Alloy Compd.*, *484* (2009) 467.
18. J. C. Chen, C. T. Hsu and C. C. Hu, *J. Power Sources*, 253 (2014) 205.
19. O. M. Magnussen, *Chem. Rev*., 102 (2002) 679.
20. C. Wang, H. Daimon, T. Onodera, T. Koda and S. Sun, *Angew. Chem. Int. Ed. Engl*., 47 (2008) 3588.
21. Z. A. Hu, Y. L. Xie, Y. X. Wang, L. J. Xie, J. L. Fu, G. R. and X. Q. Jin, *J. Phys. Chem.* C, 113 (2009).
22. M. East, *Pure. Appl. Chem*., 38 (2011) 25.
23. T. Yan, Z. Li, R. Li, Q. Ning, H. Kong, Y. Niu, *J. Mater. Chem*., *22* (2012) 23587.
24. X. Chen, X. Chen, F. Zhang, Z. Yang and S. Huang, *J. Power Sources*, 243 (2013) 555.
25. X. Sun, G. Wang, H. Sun, F. Lu, M. Yu and J. Lian, *J. Power Sources*, 238 (2013) 150.
26. H. Chen, J. Jiang, L. Zhang, T. Qi, D. Xia, H. Wan, *J. Power Sources*, 248 (2014) 28.
27. W. Sun, X. Rui, M. Ulaganathan, S. Madhavi, Q. Yan, *J. Power Sources*, *295*(2015) 323.